JIP3 links lysosome transport to regulation of multiple components of the axonal cytoskeleton

Rafiq, N.M.[1,2,3,4], Lyons, L.L. [1,2,3,4], Gowrishankar, S.[1,2,3,4,*], De Camilli, P.[1,2,3,4†] and Ferguson, S.M. [1,2,3†]

Departments of Cell Biology[1] and Neuroscience[2], Program in Cellular Neuroscience, Neurodegeneration and Repair[3], Howard Hughes Medical Institute[4], Kavli Institute for Neuroscience[4], Yale University School of Medicine, New Haven, Connecticut 06510, USA;

* present address: Department of Anatomy and Cell Biology, University of Illinois at Chicago, Chicago, Illinois 60612, USA

[†]Correspondence: shawn.ferguson@yale.edu; pietro.decamilli@yale.edu

Running title: JIP3-dependent regulation of the axonal cytoskeleton

Abstract

Lysosome axonal transport is important for the clearance of cargoes sequestered by the endocytic and autophagic pathways. Building on observations that mutations in the JIP3 (*MAPK8IP3*) gene result in lysosome-filled axonal swellings, we analyzed the impact of JIP3 depletion on the cytoskeleton of human neurons. Dynamic focal lysosome accumulations were accompanied by disruption of the axonal periodic scaffold (spectrin, F-actin and myosin II) throughout each affected axon. Additionally, axonal microtubule organization was locally disrupted at each lysosome-filled swelling. This axonal microtubule disorganization in JIP3 KO neurons was accompanied by increased tau abundance and phosphorylation. These results indicate that transport of axonal lysosomes is integrated into a much larger network that is required for the maintenance of the axonal cytoskeleton. These findings have potential relevance to human neurological disease arising from JIP3 mutations as well as for neurodegenerative tauopathies such as Alzheimer's disease.

Introduction

Neurons face major demands arising from their extreme size, polarity and longevity. Axons in particular stand out due to their length which requires both long-range transport for delivery of cargoes to and from distant locations combined with mechanisms to ensure structural integrity (Hammarlund et al., 2007; Lorenzo et al., 2019; Maday et al., 2014). These challenges create unique vulnerabilities that are reflected in the numerous neurodevelopmental and neurodegenerative diseases that arise due to defects in axonal transport and maintenance (Coleman and Hoke, 2020; Millecamps and Julien, 2013; Sleigh et al., 2019). The unique morphology and functions of axons requires specialized organization of multiple cytoskeletal components. Axonal microtubules which provide the tracks on which motors can transport organelles and other cargoes over long distances are polarized with their plus ends towards the distal axon and regulated by the binding of various microtubule binding proteins (Barnes and Polleux, 2009; Dent and Gertler, 2003; Kapitein and Hoogenraad, 2011; Stiess and Bradke, 2011). Additionally, the membrane associated periodic actin-spectrin lattice provides structural support to ensure axon integrity while non-muscle myosin II-dependent contractility coordinates the passage of organelles through the narrow confines of axons (Costa et al., 2020; Krieg et al., 2014; Vassilopoulos et al., 2019; Wang et al., 2019).

The vast majority of axonal proteins are synthesized in the neuronal cell body and proximal dendritic regions, and are subsequently transported into axons to meet their structural, signaling and metabolic demands and to support synaptic transmission (McEwen and Grafstein, 1968). Conversely, efficient retrograde transport from the axon periphery back to the cell body is required for the clearance of old or damaged proteins, as well as of material taken up by endocytosis, via endocytic and autophagic pathways (Ferguson, 2018; Kulkarni et al., 2018). This transport is primarily mediated by immature lysosomes and auto-lysosomes, which have a low content of lysosomal hydrolases and whose fate is to mature into fully degradative lysosomes in cell bodies by fusing with hydrolases-enriched vesicles delivered from the trans-Golgi network (Ferguson, 2018). The massive accumulation of these organelles at the distal side of focal blocks of

axonal transport reveals that such lysosomes are the major retrograde axonal cargo (Tsukita and Ishikawa, 1980).

A similar build-up of immature lysosomes is observed in axon swellings surrounding amyloid Aβ deposits at Alzheimer's disease amyloid plaques (both in human patients and in mouse models of the disease), which are putative sites of APP processing (Blazquez-Llorca et al., 2017; Gowrishankar et al., 2015; Nixon, 2005). A link between accumulation of axonal lysosomes due to their impaired transport and amyloidogenic APP processing was further supported by studies of neurons and mice with loss of JIP3 function (Gowrishankar et al., 2017). JIP3 is a motor interacting protein which is preferentially expressed in neurons that potentially couple cargos such as lysosomes to dynein, the microtubule minus-end directed motor (Vilela et al., 2019). JIP3 loss-of-function mutations in multiple animal species result in the build-up of lysosomes within axons (Drerup and Nechiporuk, 2013; Edwards et al., 2013; Gowrishankar et al., 2017). For example, primary cultures of mouse JIP3 knockout neurons exhibit a striking increase in the overall abundance of axonal lysosomes with focal accumulations within axonal swellings that are strikingly similar to the lysosome-filled axonal swellings observed at amyloid plaques (Gowrishankar et al., 2017). The changes in axonal morphology that accompany lysosome accumulations in JIP3 KO neurons raised questions about the relationship between lysosomes and the axonal cytoskeleton with potential implications for Alzheimer's disease.

To address these questions, we used human JIP3 KO iPSC-derived cortical glutamatergic neurons that we recently established as a cellular model for investigating the impact of JIP3 depletion on neuronal cell biology (Gowrishankar et al., 2020). Surprisingly, we found that axons with lysosome-filled swellings had a massive disruption in their actin-spectrin and myosin-II lattice organization that was not restricted to just the local site of the swelling but which occurred throughout each affected JIP3 KO axon. The additional KO of JIP4 further enhanced this phenotype, consistent with an overlapping role of the two proteins, (Gowrishankar et al., 2020). Axonal swellings filled with lysosomes were not static but formed and resolved over the course of several hours. Intriguingly, their formation coincided with local microtubule disorganization. These changes were

accompanied by a major increase in the phosphorylation of tau, a microtubule associated protein whose aberrant phosphorylation and aggregation is tightly linked to neurodegenerative disease. Our observations support a model wherein perturbed axonal lysosome transport induced by loss of JIP3 (or JIP3 and JIP4) is closely linked to a broad disruption of the neuronal cytoskeleton. These results furthermore suggest a relationship between axonal transport of lysosomes and behavior of the tau protein with potential relevance to tau-linked neurodegenerative diseases.

Results

Global disruption of the membrane periodic skeleton in axons with lysosome-filled axonal swellings

The axonal plasma membrane is supported by an organized cytoskeletal network containing actin filaments and spectrin tetramers (Han et al., 2017; He et al., 2016; Vassilopoulos et al., 2019).This actin-spectrin network, which has been linked to axonal mechanical stability (Hammarlund et al., 2007; Krieg et al., 2014) and signaling (Zhou et al., 2019), was most recently shown to undergo transient local expansion to facilitate the transport of large cargoes in narrow axons (Wang et al., 2020). The important role of this cytoskeletal scaffold in controlling axon diameter suggested that lysosome-filled axonal swellings of JIP3 KO neurons might require major rearrangement to this network. To address this question, human induced pluripotent stem cells (iPSCs) which can be differentiated into layer 2/3 cortical glutamatergic neurons (i^3Neurons) (Fernandopulle et al., 2018; Gowrishankar et al., 2020). The KO of JIP3 in this human i^3Neuron model system robustly develops lysosome-filled axonal swellings similar to those observed in primary cultures of mouse JIP3 KO cortical neuron while overcoming practical challenges arising from the neonatal lethality in the JIP3 KO mouse model (Figure 1A-C) (Gowrishankar et al., 2020; Gowrishankar et al., 2017).

We next tested whether the axons of i^3Neurons develop a membrane associated periodic skeleton similar to that observed in rodent neuron primary culture models (He et al., 2016; Xu et al., 2013). Stimulated Emission Depletion (STED) super-resolution fluorescence microscopy of control i^3Neurons after labeling with

antibodies against the C-terminus of βII-spectrin, revealed a periodic spectrin lattice (180-200nm intervals) (Figure 1D-F), in agreement with previous studies in other neuron culture systems (Xu et al., 2013; Zhong et al., 2014). In the control i^{3}Neurons, this periodic spectrin organization was apparent by 9 days of differentiation and then persisted as the neurons aged (out to 21 days in this study; Figure 1D and Supplementary Figure 1A). This lattice was also observed in JIP3 KO neurons by 9 days of differentiation, a stage at which they have undergone extensive axon growth but do not yet display lysosome accumulations (Supplementary Figure 1A). In contrast, in older JIP3 KO i^{3}Neurons that developed lysosome-filled axonal swellings, the axonal spectrin lattice was disrupted (Figure 1G-I). This striking disruption was not limited to the local site of lysosome accumulation but occurred throughout the entire affected axon (Figure 1G-I). This phenotype was even observed in axons with very sparse swellings (Supplementary Figure 1B). No difference was observed in the levels of βII-spectrin between WT and JIP3 KO neurons (Figure 1J and K). This suggested a defect in organization of βII-spectrin rather than in its synthesis. Consistent with the disruption of the spectrin periodic skeleton, the periodic organization of axonal F-actin was also lost and F-actin instead accumulated at the swellings (Figure 1L and M). Collectively, this data indicates that the actin-spectrin lattice still formed in JIP3 KO axons but then disassembled in parallel with the development of lysosome accumulations.

Non-muscle myosin-II associates with F-actin within the actin-spectrin lattice and controls axon radial contractility (Costa et al., 2020; Wang et al., 2020). We therefore examined the impact of the absence of JIP3 on the sub-cellular localization of myosin-II (Figure 1L and M). In control i^{3}Neurons, myosin-II filaments displayed a periodic pattern with occasional gaps along the axonal shaft (Figure 1L). This periodicity was completely lost in the axons of JIP3 KO i^{3}Neurons that had lysosome-filled axonal swellings (Figure 1M). In these axons, the myosin-II signal, like F-actin, was instead most prominent within the swellings.

Lysosome-filled axonal swellings coincide with sites of abnormal microtubules organization

The assembly of the actin/spectrin-based axonal periodic scaffold is dependent on intact microtubules (Zhong et al., 2014). Given the drastic disruption of this scaffold in the swollen axons of JIP3 KO i^{3}Neurons (as well as the essential role for microtubules in long range axonal transport of organelles), we next investigated microtubule organization. Remarkably, the sites at which lysosomes accumulate in JIP3 KO axons coincided with local disorganization of microtubules, as assessed by α-tubulin immunofluorescence (Figure 2A-C). The disorganization of microtubules was further exacerbated in older JIP3 KO i^{3}Neurons (Figure 2D-F). The majority of microtubules within the swellings were bent and looped, while axonal regions immediately adjacent to the swellings contained microtubules that were organized in the typical parallel bundles of control axons (Figure 2B). This disruption of the normal parallel arrangement of microtubules throughout axons was even more striking in cultures of JIP3+JIP4 double KO i^{3}Neurons, where, as previously reported (Gowrishankar et al., 2020), lysosome-filled swellings were larger and more abundant (Figure 2G-I).

Microtubules undergo several distinct post-translational modifications (Baas et al., 1993; Baas and Black, 1990; Nirschl et al., 2017), which reflect microtubule age and the activities of multiple tubulin-modifying enzymes (Janke and Magiera, 2020; Park and Roll-Mecak, 2018). Immunofluorescent labeling revealed acetylation of axonal microtubules in both control and JIP3 KO i^{3}Neurons, and there were no noticeable differences in the acetylation status of looped versus parallelly-organized microtubules in the KO neurons (Figure 3A-C). In contrast, when microtubule tyrosination status was examined, the looped microtubules were found to be predominantly detyrosinated (Figure 3D-F). The mechanisms that underlie the relationship between looping and detyrosination of microtubules remain uncertain. However, CAP-Gly domain containing proteins, such as the p150^{Glued} subunit of dynactin, prefer detyrosinated microtubules and detyrosinated microtubules have been proposed to be preferred tracks for initiating movement of axonal LAMP1-positive organelles (lysosomes) (Nirschl et al., 2016; Peris et al., 2006).

Axonal swellings are highly dynamic

We next performed long-term live cell imaging of lysosomes and microtubules in JIP3 KO i^{3}Neurons to examine the dynamics of the axonal swellings. For the

purpose of microtubule visualization, we employed low concentrations of the SiR-tubulin dye. This probe yielded a fluorescent microtubule pattern highly similar to the pattern of anti-α tubulin immunofluorescence (Figure 2A and B) including the appearance of microtubule loops within axonal swellings (Figure 2B, Figure 2D and E). Time-lapse imaging of JIP3 KO neurons stably expressing LAMP1-GFP (lysosome marker) and labeled with low concentrations of SiR-tubulin revealed that lysosome-filled axonal swellings form and resolve over a time scale of several hours (3.77 ± 1.71 hours; Figure 4A-D, Supplementary Movie S1). The close spatial and temporal relationship that was observed between lysosome accumulation and microtubule looping within these axonal swellings prevented definitive conclusions regarding a cause-effect relationship between these events (Figure 4B and C).

Lysosome-filled axonal swellings near amyloid plaques are a defining feature of Alzheimer's disease brain pathology that were exacerbated following partial depletion of JIP3 in a mouse model of the disease (Gowrishankar et al., 2017). Based on our discovery of a close spatial and temporal relationship between lysosome accumulations and disruption of the actin/spectin and microtubule cytoskeleton in JIP3 KO neurons, we wondered whether these findings could have any relevance for microtubule related aspects of Alzheimer's disease brain pathology. A hallmark of Alzheimer disease is the presence of hyperphosphorylated tau (De Strooper and Karran, 2016), a microtubule-associated protein that links microtubules to actin (Cabrales Fontela et al., 2017). Thus, we measured total tau levels as well as the phosphorylation states of sites (Thr181, Ser202/205, Ser396) that exhibit increased phosphorylation in Alzheimer disease brains. Strikingly, we found a several fold increase in total tau levels in JIP3 KO i^3Neurons and even greater increases were observed for each of the phosphorylation sites (Figure 5A-E).

Discussion

Our investigation of the relationships between lysosome axonal transport and multiple components of the axonal cytoskeleton in neurons that lack JIP3, or both JIP3 and its paralogue JIP4, revealed that focal lysosome accumulations are accompanied by major disruptions in organization of the axonal membrane associated periodic skeleton. Furthermore, the accumulation of lysosomes in focal

swellings of mutant neurons coincided both spatially and temporally with local microtubule disorganization. These observations reveal major unexpected relationships between axonal lysosome transport and the organization of multiple aspects of the axonal cytoskeleton. They furthermore raise new questions about the chain of events that link lysosome transport, microtubule organization and the cytoskeletal machinery that controls axon diameter.

Our focus on lysosomes and axonal swellings in JIP3 KO neurons was originally motivated by a wish to understand the basis for, and disease impacts of, lysosome accumulations within axonal swellings at Alzheimer's disease amyloid plaques (Gowrishankar et al., 2017; Gowrishankar et al., 2015). These efforts build on forward genetic screens in *C. elegans* and zebrafish which identified JIP3 homologs as important regulators of axonal lysosome abundance (Drerup and Nechiporuk, 2013; Edwards et al., 2013). The ability of JIP3/4 to interact with components of both kinesin and dynein motors raises the possibility that they directly control the transport of axonal organelles (Arimoto et al., 2011; Byrd et al., 2001; Cavalli et al., 2005; Huang et al., 2011; Sato et al., 2015; Sun et al., 2011; Watt et al., 2015). Their role in lysosome transport is supported both by KO phenotypes as well as by observations of JIP3 localization to axonal lysosomes (Drerup and Nechiporuk, 2013; Gowrishankar et al., 2017). Although the mechanism for JIP3 association with lysosomes has not been definitively established, JIP3 contains a modular series of protein-protein interaction domains that provide clues about how this might occur. In particular, JIP3 and JIP4 contain Rab-interacting lysosomal protein (RILP) homology 1 and 2 (RH1 and RH2) domains (Vilela et al., 2019). The RH1 domain of RILP interacts with motors (kinesin heavy chain and dynein light intermediate chain) while the RH2 domain of RILP acts as an effector of the endolysosomal small GTPase Rab7 (Johansson et al., 2007; Tan et al., 2011). By acting as a bridge between late endosomes/lysosomes and dynein-dynactin, RILP strongly promotes the movement of these organelles towards microtubule minus ends (Johansson et al., 2007; Jordens et al., 2001). JIP4 has also been linked to the dynein-dependent movement of lysosomes in non-neuronal cells via an interaction with TMEM55B, an integral membrane protein of lysosomes (Willett et al., 2017), and more recently to the budding from lysosomes in partnership with LRRK2 (Bonet-Ponce et al., 2020). The strong relationship between JIP3, JIP4 and the motility of lysosomes suggests that

the many phenotypes arising from JIP3+4 depletion arise as a consequence of a failure to efficiently move axonal lysosomes.

Although impacts of JIP3 depletion on axonal lysosome abundance have been observed in multiple species (Drerup and Nechiporuk, 2013; Edwards et al., 2013; Gowrishankar et al., 2017), broader effects of JIP3 mutation on the axonal abundance of multiple organelles have also been reported (Brown et al., 2009; Byrd et al., 2001; Noma et al., 2017; Sato et al., 2015; Sure et al., 2018). Our new observations of the dramatic cytoskeleton disruption that correlates with focal lysosome accumulations in both JIP3 KO (and JIP3+JIP4 double KO) neurons provide a potential explanation for the broad requirement for JIP3/4 for the axonal transport of multiple organelles that would not require a direct involvement of JIP3/4 in the transport of each class of organelles.

The focal accumulation of lysosomes coincides spatially and temporally with local disorganization of microtubules in JIP3 KO i^3Neurons and the overall severity of this phenotype is further exacerbated in the JIP3+JIP4 double KO neurons. Our initial expectation was that lysosome-filled swellings reflected the accumulation of lysosomes that had fallen off their microtubule tracks due to a loss of JIP3+4-dependent connections to motors. The surprising discovery that these sites of lysosome accumulation were accompanied both spatially and temporally with extensive looping of microtubules suggests a more complex relationship between lysosome transport and microtubule organization.

It was particularly striking that the dynamic formation of local axonal swellings with lysosome accumulation and microtubule looping in JIP3 KO neurons was accompanied by a widespread disruption of the integrity of the axonal membrane-associated periodic skeleton. This all-or-none effect is consistent with two distinct interpretations. One is that the focal swellings elicit changes that are propagated along the entire axonal shaft. Another is that loss of JIP3 results in an age-dependent disruption of the periodic actin/spectrin based scaffold that facilitates formation of the focal swellings where lysosomes accumulate. Interestingly, the assembly of the axonal membrane associated periodic skeleton is dependent on microtubule integrity (Qu et al., 2017; Zhong et al., 2014), suggesting that the

cytoskeletal changes observed in JIP3+JIP4 KO neurons may be interconnected. Interaction between the periodic membrane skeleton and microtubules may occur via several linker proteins, including ankyrins, which bind both spectrin and microtubules (Bennett and Davis, 1981; Leterrier et al., 2011; Zhong et al., 2014). The elucidation of the precise sequence of events will require further experimentation.

The phenotypes that we observed in JIP3 KO axons are reminiscent of axonal beading that arises in response to multiple forms of axonal perturbation (Bar-Ziv et al., 1999; Fernandez and Pullarkat, 2010; Kilinc et al., 2009). It was recently shown that changes in the local tension of the axonal membrane leads to the propagation of such “beads” (Datar et al., 2019). Myosin-II filaments within the periodic membrane skeleton contribute to contractility and may control tension homeostasis along the axonal shaft (Wang et al., 2020). Hence, if the dilations are upstream events, the all-or-none disruption of the axonal periodic scaffold within swollen JIP3 KO axons may be a consequence of tensional instability along the axons.

Loss of JIP3 could also have signaling consequences that could propagate beyond its direct subcellular site of action. In addition to interactions with motors, JIP3 (and JIP4) also intersect with signaling in the JNK pathway by acting as a scaffold that regulates the subcellular position and activity of DLK and JNK (Drerup and Nechiporuk, 2013; Ghosh et al., 2011; Kelkar et al., 2000; Kulkarni et al., 2019). Additionally, transport defects could impede the ability of lysosomes to act as sites for nutrient and growth factor-dependent activation of the mTORC1 signaling pathway (Ferguson, 2015; Liu and Sabatini, 2020).

Finally, JIP3 KO i^{3}Neurons showed a large increase in the total levels of tau and even more so in the phosphorylation of multiple sites on tau that exhibit hyper-phosphorylation in neurodegenerative diseases such as Alzheimer’s disease and frontotemporal dementia (Congdon and Sigurdsson, 2018; Edwards, 2019; Grundke-Iqbal et al., 1986; Long and Holtzman, 2019). How JIP3 mutations lead to the increases in tau levels and phosphorylation on multiple sites remains to be determined. Changes in tau phosphorylation could be directly related to cytoskeletal changes that we have observed (either of the actin/spectrin cytoskeleton or of microtubules) but may also reflect a more general response to neuronal stress

(Falzone et al., 2010; Falzone et al., 2009). It is nonetheless of great interest that reduced JIP3 expression leads to both increased Aβ production (Gowrishankar et al., 2020; Gowrishankar et al., 2017) and tau phosphorylation, two pathological hallmarks of Alzheimer's disease brain pathology.

In conclusion, our findings have revealed new reciprocal interrelations between lysosome transport and the structure and the dynamics of the axonal cytoskeleton. The stalling of lysosomes during their retrograde journey correlated with profound changes in axons. A priority for future work will be to determine cause-effect relationships between the multiple tightly linked changes that we have observed here. In addition to advancing our knowledge about fundamental aspects of cell function, these studies may provide new insight into mechanisms relevant to Alzheimer's disease pathology.

Materials and Method

Human iPSC culture and neuronal differentiation

Human iPSCs were differentiated into cortical i^{3}Neurons according to a previously described protocol based on the doxycycline inducible expression of Ngn2 (Fernandopulle et al., 2018). Briefly, the iPSCs were cultured on human embryonic stem cell (hESC)-qualified Matrigel (Corning) and fed with fresh mTeSR™1 medium (STEMCELL Technologies) on alternate days. Rho-kinase (ROCK) inhibitor Y-27632 (EMD Millipore, 10 μM) was added to the iPSC cultures on the first day of plating and replaced with fresh media without ROCK inhibitor on the following day. For neuronal differentiation, iPSCs were dissociated with Accutase (STEMCELL Technologies) and re-plated at a density between 1.5-3 x10^5 cells on matrigel-coated dishes in induction medium (KnockOut DMEM/F-12 (Thermo Fisher Scientific) containing 1% N2-supplement [Gibco], 1% NEAA [Gibco], 1% GlutaMAX [Gibco]) and 2 μg/mL doxycycline [Sigma]). After 3 days, pre-differentiated i^{3}Neurons were dispersed using Accutase and plated on poly-L-ornithine (Sigma, 1 μg/ml) and laminin (Thermo Fisher Scientific, 10 μg/ml) coated 35 mm glass-bottom dishes (MatTek) or 6-well plates (Corning) for imaging and immunoblotting, respectively. These i^{3}Neurons were cultured and maintained in cortical medium (induction medium supplemented with 2% B27 (Gibco), 10 ng/mL BDNF (PeproTech), 10 ng/mL NT-3 (PeproTech) and 1 μg/mL laminin). Fresh cortical media was added to the existing media every 5 days. The iPSCs and i^{3}Neurons were kept at 37ºC with 5% CO_2 in an enclosed incubator.

Live cell imaging

Live imaging of control, JIP3 KO and JIP3+4 KO i^{3}Neurons (Gowrishankar et al., 2020) was performed on day 10-22 post-differentiation in cortical medium supplied with 5% CO_2 and maintained at 37ºC. I^{3}Neurons stably-expressing LAMP1-GFP (Gowrishankar et al., 2020) or LysoTracker-labelled i^{3}Neurons were used to visualize lysosome dynamics. For lysotracker labeling, i^{3}Neurons were stained with 30 nM LysoTracker™ Green DND-26 or 10 nM LysoTracker™ Deep Red (Thermo Fisher Scientific) for 3 mins, washed twice with fresh cortical media, and then imaged immediately.

Immunofluorescence

For i^{3}Neuron samples involving actin and spectrin staining, cells were fixed and extracted for 1 minute using a solution of 0.3% (v/v) glutaraldehyde and 0.25% (v/v) Triton X-100 in cytoskeleton buffer (CB, 10 mM MES pH 6.1, 150 mM NaCl, 5 mM EGTA, 5 mM glucose and 5 mM $MgCl_2$), post-fixed for 15 min in 2% (v/v) glutaraldehyde in CB at 37ºC, and then washed twice in phosphate-buffered saline (PBS) according to previously described protocol (Xu et al., 2013). For microtubule staining, cells were fixed and extracted for 15 minutes using a solution of 4% (v/v) paraformaldehyde, 0.2% (v/v) glutaraldehyde and 0.25% (v/v) Triton X-100 in CB at 37ºC, and then washed twice in PBS. For removal of free aldehyde groups, cells were quenched with fresh 1 mg/ml sodium borohydride in CB (Sigma) for 10 mins, and then washed thrice in PBS. Cells were further blocked for 30 minutes in 5% bovine serum albumin (BSA, Sigma) in phosphate-buffered saline (PBS) and then incubated overnight at 4ºC with the following appropriate antibodies: anti-α-tubulin (Sigma, catalogue no. T6199, dilution 1:500); anti-LAMP1 (Cell Signaling Technology, catalogue no. 9091, dilution 1:500) or (Developmental Studies Hybridoma Bank, clone 1D4B, dilution 1:500); anti-βII-spectrin (BD Transduction Laboratories, Clone 42/B-Spectrin II, dilution 1:250); anti-non muscle heavy chain of myosin-IIA (Sigma, catalogue no. M8064, dilution 1:500); anti-acetyl α-tubulin (Cell Signaling Technology, catalogue no. 5335, dilution 1:250); anti-detyrosinated α-tubulin (Abcam, catalogue no. ab48389, dilution 1:250); anti-tyrosinated α-tubulin (Millipore Sigma, clone YL1/2, dilution 1:250). Cells were washed with PBS thrice and incubated with Alexa Fluor-conjugated secondary antibodies (Thermo Fisher Scientific) for 1 hour at room temperature, followed by three washes in PBS. F-actin was visualized by Alexa Fluor 488 or rhodamine-conjugated phalloidin (Thermo Fisher Scientific, dilution 1:100).

Immunoblotting

Control, JIP3 KO and JIP3+4 KO i^{3}Neurons were grown on six-well plates (3 x 10^5 cells/well). After post-differentiation in cortical media, i^{3}Neurons (typically 17 days post-differentiation) were washed with ice-cold PBS and then lysed in lysis buffer (50 mM Tris pH 7.4, 150 mM NaCl, 1 mM EDTA, and 1% Triton X-100) supplemented with cOmplete™ EDTA-free protease inhibitor cocktail (Roche) and PhosSTOP phosphatase inhibitor cocktail (Roche), followed by centrifugation at 13,000xg for 6

min. The supernatant was collected and incubated at 95°C for 5 min in SDS sample buffer containing 1% 2-mercaptoethanol (Sigma). The extracted proteins were separated by SDS-PAGE in Mini-PROTEAN TGX precast polyacrylamide gels (Bio-Rad) and transferred to nitrocellulose membranes (Bio-Rad) at 100V for 1 hour or 75V for 2 hours (for high molecular weight proteins: >150kDa). Subsequently, the nitrocellulose membranes were blocked for 1 hour with 5% non-fat milk (AmericanBIO) in TBST (tris-buffered saline [TBS] + 0.1% tween 20), then incubated overnight at 4ºC with primary antibodies: anti-JIP3 (Novus Biologicals, catalogue no. NBP1-00895, dilution 1:500); anti-JIP4 (Cell Signaling Technology, catalogue no. 5519, dilution 1:1000); anti-S6 Ribosomal Protein (RS6, Cell Signaling Technology, catalogue no. 2217, dilution 1:2500); anti-βII-spectrin (BD Transduction Laboratories, Clone 42/B-Spectrin II, dilution 1:1000); anti-tau (Tau46, Cell Signaling Technology, catalogue no. 4019, dilution 1:1000); anti-phospho-tau Thr181 (Cell Signaling Technology, catalogue no. 12885, dilution 1:1000); anti-phospho-tau Ser202/Thr205 (AT8, Thermo Fisher Scientific (Invitrogen), catalogue no. MN1020, dilution 1:1000); anti-phospho-tau Ser396 (Cell Signaling Technology, catalogue no. 9632, dilution 1:1000).

Subsequently, the nitrocellulose membranes were washed 3 times (10 minutes each) in TBST and probed by incubation for 1 hour with the secondary antibodies conjugated with horseradish peroxidase. The membranes were then washed three times (15 minutes at room temperature each), developed using Pierce™ ECL western blotting substratum (Thermo Fisher Scientific) and imaged by a Versa-Doc imaging system (Bio-Rad).

Fluorescence microscopy

Two types of high-resolution microscopes were used in this study. The LSM 880 inverted confocal laser scanning microscope with Airyscan (Carl Zeiss Microscopy) is accompanied with 63×/1.40 numerical aperture (NA) plan-apochromat differential interference contrast (DIC) oil immersion objective and 32-channel gallium arsenide phosphide (GaAsP)-photomultiplier tubes (PMT) area detector. 488 nm, 561 nm and 633 laser lines were used in this study. Images were acquired and processed using ZEN imaging software (Zeiss). The Leica TCS SP8 gated STED super-resolution confocal microscope (Leica Microsystems) is coupled with Leica harmonic

compound (HC) plan apochromatic (PL APO) 100×/1.40 oil STED objective and Leica gated HyD hybrid detector. Briefly, A white light excitation laser accompanied with 592 nm, 660 nm and 775 nm depletion lasers were used in this study. Images were acquired using LAS X software (Leica Microsystems) and final images were deconvolved using Huygens deconvolution software (Huygens Essentials, Scientific Volume Imaging).

Quantification and statistical analysis

Images were pseudocolor-coded, adjusted for brightness and contrast, cropped and/or rotated using the open-source image processing software FIJI (ImageJ) (Schindelin et al., 2012). Dendrites and axons were identified by visual tracking of the length of the neurite. Percentage of neurites were quantified using the FIJI plugin "NeuronJ" and/or the FIJI segmented lines + ROI manager tool to determine the total number of neurites. Western blot data were processed using Image Lab software (Bio-Rad) and quantified using the "Gels" ImageJ plugin. The methods for statistical analysis and sizes of the samples (n) are specified in the results section or figure legends for all of the quantitative data. Student's t test or Mann-Whitney test was used when comparing two data sets. Differences were accepted as significant for $P < 0.05$. Prism version 8 (GraphPad Software) was used to plot, analyze and represent the data.

Acknowledgements

We are grateful to Michael Ward (NINDS) for his contribution of the human iPSCs with doxycycline-inducible Ngn2 expression and his generous advice on their use. This research was supported in part by the Dementia Discovery Foundation (SMF and PDC), the NIH (NS36251 to PDC; AG062210 TO SMF), and the Kavli Foundation (PDC). The authors do not have any conflicts to declare.

Author contributions

NBMR and LLL designed and performed all experiments. SG developed key reagents. NBMR, SMF and PDC discussed results and prepared the manuscript.

Figure Legends

Figure 1: Lysosome-filled axonal swellings in JIP3 KO axons correlate with global disruption of the membrane periodic skeleton

(A and B) Airyscan imaging of control i^{3}Neurons and JIP3 KO i^{3}Neurons (13 days of differentiation). Yellow arrowheads highlight lysosome-positive axonal swellings in the KO neurons (scale bars, 15 μm). (C) Percentage of i^{3}Neurons containing at least one lysosome-positive axonal swelling represented as mean ± SD, pooled from four independent experiments (n≥32 per experiment, 13 days of differentiation). (D and E) STED microscopy images of βII-spectrin immunofluorescence in the axons of control i^{3}Neurons (day 17). (Scale bars, E: 5 μm; F: 1 μm). (F) Graph demonstrating the longitudinal distance between peaks in the βII-spectrin signal from the boxed region in (E). (G) Airyscan microscopy images of control i^{3}Neurons show regular distribution of lysosomes (LAMP1, white) and intact periodic membrane skeletons (βII-spectrin, green). (H) JIP3 KO i^{3}Neurons (day 15) exhibit disruption in the spectrin periodicity in axons positive for lysosome accumulations (scale bars, 5 μm). (I) Percentage of swollen axons with disrupted periodic membrane skeleton represented as mean ± SD pooled from three independent experiments (≥20 axons analyzed per experiment). Lysosomes and the periodic membrane skeleton were labeled with LAMP1 and βII-spectrin antibodies, respectively. (J and K) Immunoblot showing levels of βII-spectrin in control and JIP3 KO i^{3}Neurons (day 15); ribosomal protein S6 was used as loading control (J), and their normalized expression levels is shown in (K). (L) STED microscopy images of myosin-II filaments (green) show a periodic distribution similar to that of F-actin (magenta) in control i^{3}Neurons. (M) Myosin-II and actin periodicity is lost in JIP3 KO i^{3}Neurons (day 15) and both were enriched at the lysosome-positive axonal swellings (white). Lysosomes and myosin-II filaments were labeled with antibodies against LAMP1 and non-muscle myosin-IIA respectively, while rhodamine phalloidin was used to label F-actin. Scale bars, 5 μm. p-values were calculated using two-tailed Student's t-test.

Figure 2: Lysosome-filled axonal swellings in JIP3 KO axons coincide with sites of abnormal microtubule organization

(A and B) Airyscan imaging of LAMP1 (green) and α-tubulin (magenta) immunofluorescence in control and JIP3 KO neurons (day 13) respectively (scale bars, 5 μm). (C) Percentage of swollen axons with abnormally looped microtubules presented (mean ± SD; pooled from three independent experiments, ≥30 axons per experiment). (D-E) Control and JIP3 KO neurons after 22 days of differentiation labeled for microtubules (SiR-tubulin; yellow arrowheads highlight examples of severe microtubule looping; scale bars, 5 μm). (F) The percentage of neurites (mean ± SD) with disorganized microtubules pooled from four independent experiments of 22 day old cultures (≥34 neurites per experiment). (G and H) Lysotracker (green) and SiR-Tubulin (magenta) in control and JIP3+JIP4 double KO neurons (day 12) respectively (scale bars, 5 μm). (I) The percentage of neurites (mean ± SD) with disorganized microtubules pooled from four independent experiments (≥22 neurites per experiment). p-values in all experiments were calculated using two-tailed Student's t-tests.

Figure 3: Microtubule loops in JIP3 KO axonal swellings are primarily detyrosinated

(A and B) Airyscan microscopy images of acetylated-α-tubulin, (green) and total microtubules (magenta) in control and JIP3 KO i^{3}Neurons (day 13) respectively. Scale bars, 5 μm. (C) Fraction of acetylated and non-acetylated microtubules in JIP3 KO i^{3}Neurons (pooled data from 2 experiment with ≥19 swellings analyzed per experiment). (D and E) Airyscan microscopy images of neurites from both control (D) and JIP3 KO i^{3}Neurons (day 13) (E) consist of parallel microtubule bundles that are either detyrosinated (green) or tyrosinated (magenta) in control and JIP3 KO i^{3}Neurons respectively. Scale bars, 5 μm. (F) Fraction of detyrosinated and tyrosinated microtubules in JIP3 KO i^{3}Neurons (pooled from three independent experiments with ≥18 swellings analyzed per experiment).

Figure 4: Lysosome-positive axonal swellings are dynamic in JIP3 KO neurons

(A) Representative image of JIP3 KO i^{3}Neurons (day 15) stably expressing LAMP1-GFP (green) and labeled with SiR-tubulin (magenta) at the beginning of a 12-hour time lapse imaging time course (Airyscan microscopy). Scale bar, 5 μm. (B) Images from the boxed area in (A) at the indicated time points. Scale bar, 2 μm. (C) Kymograph of the region (marked by white line in B; scale bar, 2 hours). (D) Scatter

dot plot (mean ± SEM) depicting the duration of 41 swellings pooled from 7 independent experiments. Scale bar, 5 μm.

Figure 5: Increased tau phosphorylation levels in JIP3 KO and JIP3+JIP4 double KO neurons

(A) Immunoblots showing levels of total tau and phospho-tau at residues Ser396, Thr181 and Ser202/Thr205 (AT8) in control and JIP3 KO i^{3}Neurons (days 17-20). Ribosomal protein S6 immunoblots served as loading controls. (B-E) Quantification of total Tau levels (B, n=3 independent experiments), and phosphorylated tau levels at residues Ser396 (C, n=3), Thr181 (D, n=2) and Ser202/Thr205 (E, n=2) in control and JIP3 KO i^{3}Neurons respectively. All p-values were calculated using two-tailed Student's t-test.

Supplementary Figure 1: βII-spectrin organization in JIP3 KO i^{3}Neurons

(A) Airyscan microscopy images of young JIP3 KO i^{3}Neurons (day 9) with no lysosome-positive swellings (LAMP1, white) display intact periodic membrane skeleton (βII-spectrin, green). (B) The global disruption of the periodic membrane skeleton shown in Figure 1H is also seen in JIP3 KO i^{3}Neuron (day 13) with very sparse lysosome-positive axonal swellings. Lysosomes and the periodic membrane skeleton were labeled with LAMP1 and βII-spectrin antibodies, respectively. Scale bars, 5 μm.

Supplementary Movie 1: Dynamic formation and resolution of axonal swellings in JIP3 KO neurons

JIP3 KO iNeurons (day 15) stably expressing LAMP1-GFP were labeled with SiR tubulin to mark lysosomes and microtubules, respectively. Images were acquired at 5-minute intervals over a period of 12 hours using Airyscan microscopy. Scale bar, 5 μm. Display rate is 5 frames/sec.

References

Arimoto, M., S.P. Koushika, B.C. Choudhary, C. Li, K. Matsumoto, and N. Hisamoto. 2011. The Caenorhabditis elegans JIP3 protein UNC-16 functions as an adaptor to link kinesin-1 with cytoplasmic dynein. *J Neurosci*. 31:2216-2224.

Baas, P.W., F.J. Ahmad, T.P. Pienkowski, A. Brown, and M.M. Black. 1993. Sites of microtubule stabilization for the axon. *J Neurosci*. 13:2177-2185.

Baas, P.W., and M.M. Black. 1990. Individual microtubules in the axon consist of domains that differ in both composition and stability. *J Cell Biol*. 111:495-509.

Bar-Ziv, R., T. Tlusty, E. Moses, S.A. Safran, and A. Bershadsky. 1999. Pearling in cells: a clue to understanding cell shape. *Proc Natl Acad Sci U S A*. 96:10140-10145.

Barnes, A.P., and F. Polleux. 2009. Establishment of axon-dendrite polarity in developing neurons. *Annu Rev Neurosci*. 32:347-381.

Bennett, V., and J. Davis. 1981. Erythrocyte ankyrin: immunoreactive analogues are associated with mitotic structures in cultured cells and with microtubules in brain. *Proc Natl Acad Sci U S A*. 78:7550-7554.

Blazquez-Llorca, L., S. Valero-Freitag, E.F. Rodrigues, A. Merchan-Perez, J.R. Rodriguez, M.M. Dorostkar, J. DeFelipe, and J. Herms. 2017. High plasticity of axonal pathology in Alzheimer's disease mouse models. *Acta Neuropathol Commun*. 5:14.

Bonet-Ponce, L., A. Beilina, C.D. Williamson, E. Lindberg, J.H. Kluss, S. Saez-Atienzar, N. Landeck, R. Kumaran, A. Mamais, C.K.E. Bleck, Y. Li, and M.R. Cookson. 2020. LRRK2 mediates tubulation and vesicle sorting from membrane damaged lysosomes. *bioRxiv*:2020.2001.2023.917252.

Brown, H.M., H.A. Van Epps, A. Goncharov, B.D. Grant, and Y. Jin. 2009. The JIP3 scaffold protein UNC-16 regulates RAB-5 dependent membrane trafficking at C. elegans synapses. *Dev Neurobiol*. 69:174-190.

Byrd, D.T., M. Kawasaki, M. Walcoff, N. Hisamoto, K. Matsumoto, and Y. Jin. 2001. UNC-16, a JNK-signaling scaffold protein, regulates vesicle transport in C. elegans. *Neuron*. 32:787-800.

Cabrales Fontela, Y., H. Kadavath, J. Biernat, D. Riedel, E. Mandelkow, and M. Zweckstetter. 2017. Multivalent cross-linking of actin filaments and microtubules through the microtubule-associated protein Tau. *Nat Commun*. 8:1981.

Cavalli, V., P. Kujala, J. Klumperman, and L.S. Goldstein. 2005. Sunday Driver links axonal transport to damage signaling. *J Cell Biol*. 168:775-787.

Coleman, M.P., and A. Hoke. 2020. Programmed axon degeneration: from mouse to mechanism to medicine. *Nat Rev Neurosci*. 21:183-196.

Congdon, E.E., and E.M. Sigurdsson. 2018. Tau-targeting therapies for Alzheimer disease. *Nat Rev Neurol*. 14:399-415.

Costa, A.R., S.C. Sousa, R. Pinto-Costa, J.C. Mateus, C.D. Lopes, A.C. Costa, D. Rosa, D. Machado, L. Pajuelo, X. Wang, F. Zhou, A.J. Pereira, P. Sampaio, B.Y. Rubinstein, I. Mendes Pinto, M. Lampe, P. Aguiar, and M.M. Sousa. 2020. The membrane periodic skeleton is an actomyosin network that regulates axonal diameter and conduction. *Elife*. 9.

Datar, A., J. Ameeramja, A. Bhat, R. Srivastava, A. Mishra, R. Bernal, J. Prost, A. Callan-Jones, and P.A. Pullarkat. 2019. The Roles of Microtubules and Membrane Tension in Axonal Beading, Retraction, and Atrophy. *Biophys J*. 117:880-891.

De Strooper, B., and E. Karran. 2016. The Cellular Phase of Alzheimer's Disease. *Cell*. 164:603-615.

Dent, E.W., and F.B. Gertler. 2003. Cytoskeletal dynamics and transport in growth cone motility and axon guidance. *Neuron*. 40:209-227.

Drerup, C.M., and A.V. Nechiporuk. 2013. JNK-interacting protein 3 mediates the retrograde transport of activated c-Jun N-terminal kinase and lysosomes. *PLoS Genet*. 9:e1003303.

Edwards, F.A. 2019. A Unifying Hypothesis for Alzheimer's Disease: From Plaques to Neurodegeneration. *Trends Neurosci*. 42:310-322.

Edwards, S.L., S.C. Yu, C.M. Hoover, B.C. Phillips, J.E. Richmond, and K.G. Miller. 2013. An organelle gatekeeper function for Caenorhabditis elegans UNC-16 (JIP3) at the axon initial segment. *Genetics*. 194:143-161.

Falzone, T.L., S. Gunawardena, D. McCleary, G.F. Reis, and L.S. Goldstein. 2010. Kinesin-1 transport reductions enhance human tau hyperphosphorylation, aggregation and neurodegeneration in animal models of tauopathies. *Hum Mol Genet*. 19:4399-4408.

Falzone, T.L., G.B. Stokin, C. Lillo, E.M. Rodrigues, E.L. Westerman, D.S. Williams, and L.S. Goldstein. 2009. Axonal stress kinase activation and tau misbehavior induced by kinesin-1 transport defects. *J Neurosci*. 29:5758-5767.

Ferguson, S.M. 2015. Beyond indigestion: emerging roles for lysosome-based signaling in human disease. *Curr Opin Cell Biol*. 35:59-68.

Ferguson, S.M. 2018. Axonal transport and maturation of lysosomes. *Curr Opin Neurobiol*. 51:45-51.

Fernandez, P., and P.A. Pullarkat. 2010. The role of the cytoskeleton in volume regulation and beading transitions in PC12 neurites. *Biophys J*. 99:3571-3579.

Fernandopulle, M.S., R. Prestil, C. Grunseich, C. Wang, L. Gan, and M.E. Ward. 2018. Transcription Factor-Mediated Differentiation of Human iPSCs into Neurons. *Curr Protoc Cell Biol*. 79:e51.

Ghosh, A.S., B. Wang, C.D. Pozniak, M. Chen, R.J. Watts, and J.W. Lewcock. 2011. DLK induces developmental neuronal degeneration via selective regulation of proapoptotic JNK activity. *J Cell Biol*. 194:751-764.

Gowrishankar, S., L. Lyons, N.M. Rafiq, A. Roczniak-Ferguson, P. De Camilli, and S.M. Ferguson. 2020. Overlapping roles of JIP3 and JIP4 in promoting axonal transport of lysosomes in human iPSC-derived neurons. *bioRxiv*:2020.2006.2013.149443.

Gowrishankar, S., Y. Wu, and S.M. Ferguson. 2017. Impaired JIP3-dependent axonal lysosome transport promotes amyloid plaque pathology. *J Cell Biol*. 216:3291-3305.

Gowrishankar, S., P. Yuan, Y. Wu, M. Schrag, S. Paradise, J. Grutzendler, P. De Camilli, and S.M. Ferguson. 2015. Massive accumulation of luminal protease-deficient axonal lysosomes at Alzheimer's disease amyloid plaques. *Proc Natl Acad Sci U S A*. 112:E3699-3708.

Grundke-Iqbal, I., K. Iqbal, Y.C. Tung, M. Quinlan, H.M. Wisniewski, and L.I. Binder. 1986. Abnormal phosphorylation of the microtubule-associated protein tau (tau) in Alzheimer cytoskeletal pathology. *Proc Natl Acad Sci U S A*. 83:4913-4917.

Hammarlund, M., E.M. Jorgensen, and M.J. Bastiani. 2007. Axons break in animals lacking beta-spectrin. *J Cell Biol*. 176:269-275.

Han, B., R. Zhou, C. Xia, and X. Zhuang. 2017. Structural organization of the actin-spectrin-based membrane skeleton in dendrites and soma of neurons. *Proc Natl Acad Sci U S A*. 114:E6678-E6685.

He, J., R. Zhou, Z. Wu, M.A. Carrasco, P.T. Kurshan, J.E. Farley, D.J. Simon, G. Wang, B. Han, J. Hao, E. Heller, M.R. Freeman, K. Shen, T. Maniatis, M. Tessier-Lavigne, and X.

Zhuang. 2016. Prevalent presence of periodic actin-spectrin-based membrane skeleton in a broad range of neuronal cell types and animal species. *Proc Natl Acad Sci U S A*. 113:6029-6034.

Huang, S.H., S. Duan, T. Sun, J. Wang, L. Zhao, Z. Geng, J. Yan, H.J. Sun, and Z.Y. Chen. 2011. JIP3 mediates TrkB axonal anterograde transport and enhances BDNF signaling by directly bridging TrkB with kinesin-1. *J Neurosci*. 31:10602-10614.

Janke, C., and M.M. Magiera. 2020. The tubulin code and its role in controlling microtubule properties and functions. *Nat Rev Mol Cell Biol*.

Johansson, M., N. Rocha, W. Zwart, I. Jordens, L. Janssen, C. Kuijl, V.M. Olkkonen, and J. Neefjes. 2007. Activation of endosomal dynein motors by stepwise assembly of Rab7-RILP-p150Glued, ORP1L, and the receptor betalll spectrin. *J Cell Biol*. 176:459-471.

Jordens, I., M. Fernandez-Borja, M. Marsman, S. Dusseljee, L. Janssen, J. Calafat, H. Janssen, R. Wubbolts, and J. Neefjes. 2001. The Rab7 effector protein RILP controls lysosomal transport by inducing the recruitment of dynein-dynactin motors. *Curr Biol*. 11:1680-1685.

Kapitein, L.C., and C.C. Hoogenraad. 2011. Which way to go? Cytoskeletal organization and polarized transport in neurons. *Mol Cell Neurosci*. 46:9-20.

Kelkar, N., S. Gupta, M. Dickens, and R.J. Davis. 2000. Interaction of a mitogen-activated protein kinase signaling module with the neuronal protein JIP3. *Mol Cell Biol*. 20:1030-1043.

Kilinc, D., G. Gallo, and K.A. Barbee. 2009. Mechanical membrane injury induces axonal beading through localized activation of calpain. *Exp Neurol*. 219:553-561.

Krieg, M., A.R. Dunn, and M.B. Goodman. 2014. Mechanical control of the sense of touch by beta-spectrin. *Nat Cell Biol*. 16:224-233.

Kulkarni, A., J. Chen, and S. Maday. 2018. Neuronal autophagy and intercellular regulation of homeostasis in the brain. *Curr Opin Neurobiol*. 51:29-36.

Kulkarni, S.S., V. Sabharwal, S. Sheoran, A. Basu, K. Matsumoto, N. Hisamoto, A. Ghosh-Roy, and S.P. Koushika. 2019. UNC-16/JIP3 negatively regulates actin dynamics dependent on DLK-1 and microtubule dynamics independent of DLK-1 in regenerating neurons. *bioRxiv*:484683.

Leterrier, C., H. Vacher, M.P. Fache, S.A. d'Ortoli, F. Castets, A. Autillo-Touati, and B. Dargent. 2011. End-binding proteins EB3 and EB1 link microtubules to ankyrin G in the axon initial segment. *Proc Natl Acad Sci U S A*. 108:8826-8831.

Liu, G.Y., and D.M. Sabatini. 2020. mTOR at the nexus of nutrition, growth, ageing and disease. *Nat Rev Mol Cell Biol*.

Long, J.M., and D.M. Holtzman. 2019. Alzheimer Disease: An Update on Pathobiology and Treatment Strategies. *Cell*. 179:312-339.

Lorenzo, D.N., A. Badea, R. Zhou, P.J. Mohler, X. Zhuang, and V. Bennett. 2019. betaII-spectrin promotes mouse brain connectivity through stabilizing axonal plasma membranes and enabling axonal organelle transport. *Proc Natl Acad Sci U S A*. 116:15686-15695.

Maday, S., A.E. Twelvetrees, A.J. Moughamian, and E.L. Holzbaur. 2014. Axonal transport: cargo-specific mechanisms of motility and regulation. *Neuron*. 84:292-309.

McEwen, B.S., and B. Grafstein. 1968. Fast and slow components in axonal transport of protein. *J Cell Biol*. 38:494-508.

Millecamps, S., and J.P. Julien. 2013. Axonal transport deficits and neurodegenerative diseases. *Nat Rev Neurosci*. 14:161-176.

Nirschl, J.J., A.E. Ghiretti, and E.L.F. Holzbaur. 2017. The impact of cytoskeletal organization on the local regulation of neuronal transport. *Nat Rev Neurosci*. 18:585-597.

Nirschl, J.J., M.M. Magiera, J.E. Lazarus, C. Janke, and E.L. Holzbaur. 2016. alpha-Tubulin Tyrosination and CLIP-170 Phosphorylation Regulate the Initiation of Dynein-Driven Transport in Neurons. *Cell Rep*. 14:2637-2652.

Nixon, R.A. 2005. Endosome function and dysfunction in Alzheimer's disease and other neurodegenerative diseases. *Neurobiol Aging*. 26:373-382.

Noma, K., A. Goncharov, M.H. Ellisman, and Y. Jin. 2017. Microtubule-dependent ribosome localization in C. elegans neurons. *Elife*. 6.

Park, J.H., and A. Roll-Mecak. 2018. The tubulin code in neuronal polarity. *Curr Opin Neurobiol*. 51:95-102.

Peris, L., M. Thery, J. Faure, Y. Saoudi, L. Lafanechere, J.K. Chilton, P. Gordon-Weeks, N. Galjart, M. Bornens, L. Wordeman, J. Wehland, A. Andrieux, and D. Job. 2006. Tubulin tyrosination is a major factor affecting the recruitment of CAP-Gly proteins at microtubule plus ends. *J Cell Biol*. 174:839-849.

Qu, Y., I. Hahn, S.E. Webb, S.P. Pearce, and A. Prokop. 2017. Periodic actin structures in neuronal axons are required to maintain microtubules. *Mol Biol Cell*. 28:296-308.

Sato, T., M. Ishikawa, M. Mochizuki, M. Ohta, M. Ohkura, J. Nakai, N. Takamatsu, and K. Yoshioka. 2015. JSAP1/JIP3 and JLP regulate kinesin-1-dependent axonal transport to prevent neuronal degeneration. *Cell Death Differ*. 22:1260-1274.

Schindelin, J., I. Arganda-Carreras, E. Frise, V. Kaynig, M. Longair, T. Pietzsch, S. Preibisch, C. Rueden, S. Saalfeld, B. Schmid, J.Y. Tinevez, D.J. White, V. Hartenstein, K. Eliceiri, P. Tomancak, and A. Cardona. 2012. Fiji: an open-source platform for biological-image analysis. *Nat Methods*. 9:676-682.

Sleigh, J.N., A.M. Rossor, A.D. Fellows, A.P. Tosolini, and G. Schiavo. 2019. Axonal transport and neurological disease. *Nature Reviews Neurology*.

Stiess, M., and F. Bradke. 2011. Neuronal polarization: the cytoskeleton leads the way. *Dev Neurobiol*. 71:430-444.

Sun, F., C. Zhu, R. Dixit, and V. Cavalli. 2011. Sunday Driver/JIP3 binds kinesin heavy chain directly and enhances its motility. *EMBO J*. 30:3416-3429.

Sure, G.R., A. Chatterjee, N. Mishra, V. Sabharwal, S. Devireddy, A. Awasthi, S. Mohan, and S.P. Koushika. 2018. UNC-16/JIP3 and UNC-76/FEZ1 limit the density of mitochondria in C. elegans neurons by maintaining the balance of anterograde and retrograde mitochondrial transport. *Sci Rep*. 8:8938.

Tan, S.C., J. Scherer, and R.B. Vallee. 2011. Recruitment of dynein to late endosomes and lysosomes through light intermediate chains. *Mol Biol Cell*. 22:467-477.

Tsukita, S., and H. Ishikawa. 1980. The movement of membranous organelles in axons. Electron microscopic identification of anterogradely and retrogradely transported organelles. *J Cell Biol*. 84:513-530.

Vassilopoulos, S., S. Gibaud, A. Jimenez, G. Caillol, and C. Leterrier. 2019. Ultrastructure of the axonal periodic scaffold reveals a braid-like organization of actin rings. *Nat Commun*. 10:5803.

Vilela, F., C. Velours, M. Chenon, M. Aumont-Nicaise, V. Campanacci, A. Thureau, O. Pylypenko, J. Andreani, P. Llinas, and J. Menetrey. 2019. Structural characterization

of the RH1-LZI tandem of JIP3/4 highlights RH1 domains as a cytoskeletal motor-binding motif. *Sci Rep*. 9:16036.

Wang, G., D.J. Simon, Z. Wu, D.M. Belsky, E. Heller, M.K. O'Rourke, N.T. Hertz, H. Molina, G. Zhong, M. Tessier-Lavigne, and X. Zhuang. 2019. Structural plasticity of actin-spectrin membrane skeleton and functional role of actin and spectrin in axon degeneration. *Elife*. 8.

Wang, T., W. Li, S. Martin, A. Papadopulos, M. Joensuu, C. Liu, A. Jiang, G. Shamsollahi, R. Amor, V. Lanoue, P. Padmanabhan, and F.A. Meunier. 2020. Radial contractility of actomyosin rings facilitates axonal trafficking and structural stability. *J Cell Biol*. 219.

Watt, D., R. Dixit, and V. Cavalli. 2015. JIP3 Activates Kinesin-1 Motility to Promote Axon Elongation. *J Biol Chem*. 290:15512-15525.

Willett, R., J.A. Martina, J.P. Zewe, R. Wills, G.R.V. Hammond, and R. Puertollano. 2017. TFEB regulates lysosomal positioning by modulating TMEM55B expression and JIP4 recruitment to lysosomes. *Nat Commun*. 8:1580.

Xu, K., G. Zhong, and X. Zhuang. 2013. Actin, spectrin, and associated proteins form a periodic cytoskeletal structure in axons. *Science*. 339:452-456.

Zhong, G., J. He, R. Zhou, D. Lorenzo, H.P. Babcock, V. Bennett, and X. Zhuang. 2014. Developmental mechanism of the periodic membrane skeleton in axons. *Elife*. 3.

Zhou, R., B. Han, C. Xia, and X. Zhuang. 2019. Membrane-associated periodic skeleton is a signaling platform for RTK transactivation in neurons. *Science*. 365:929-934.

Figure 1

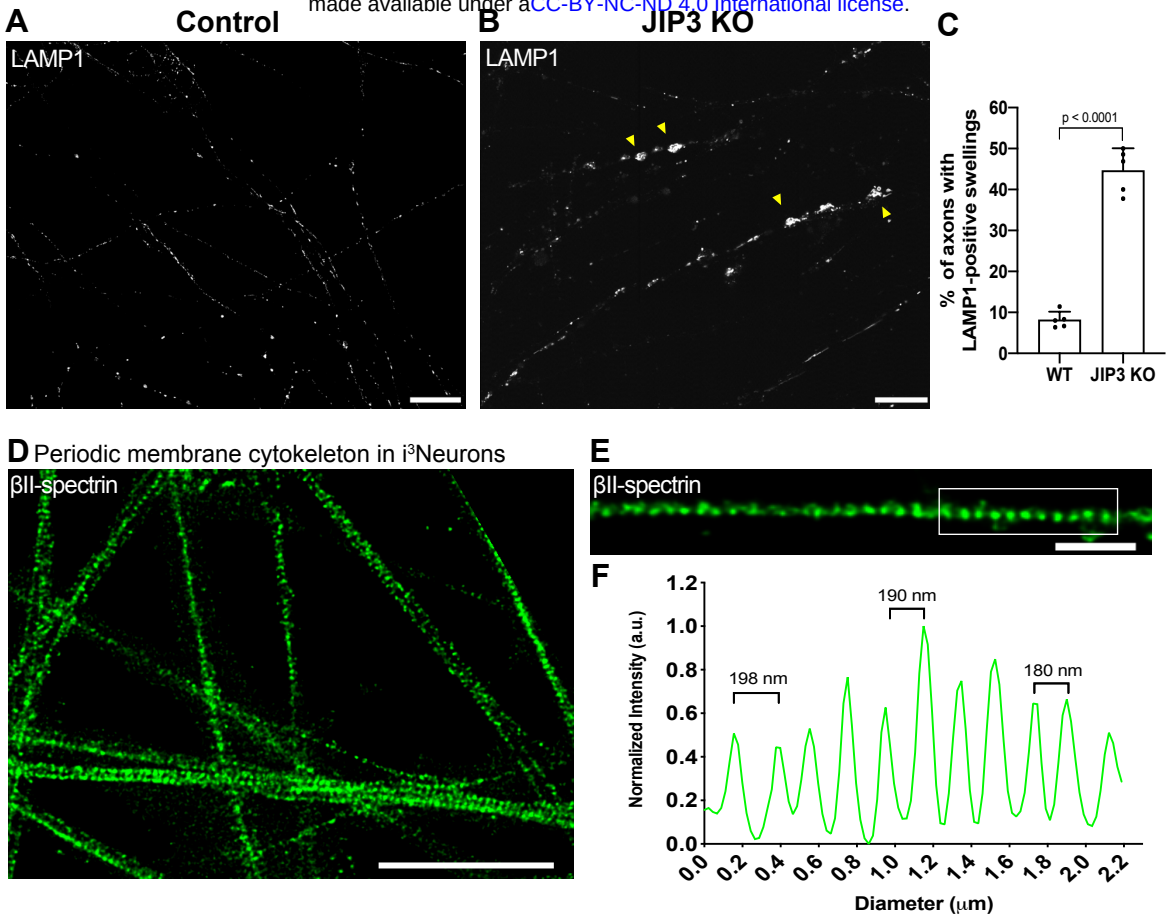

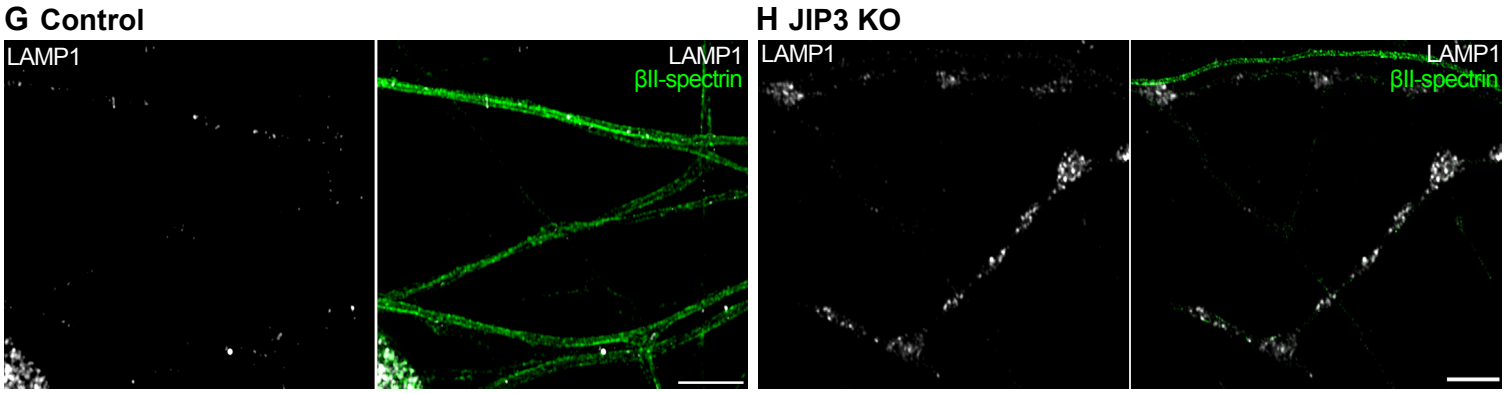

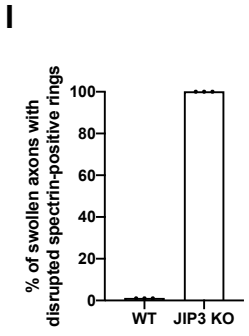

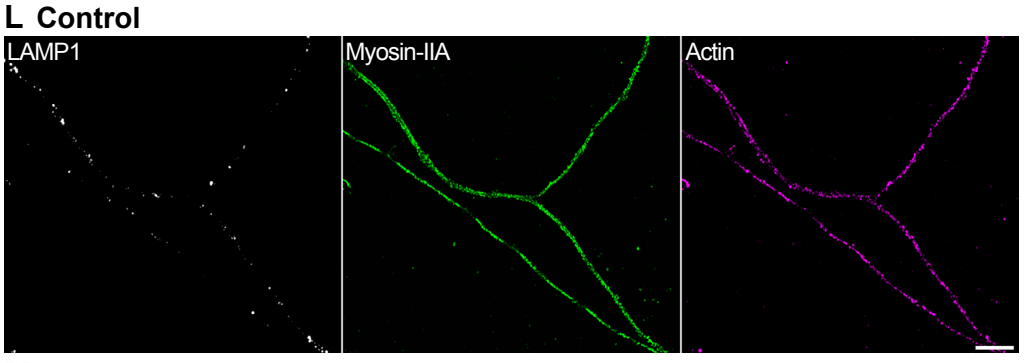

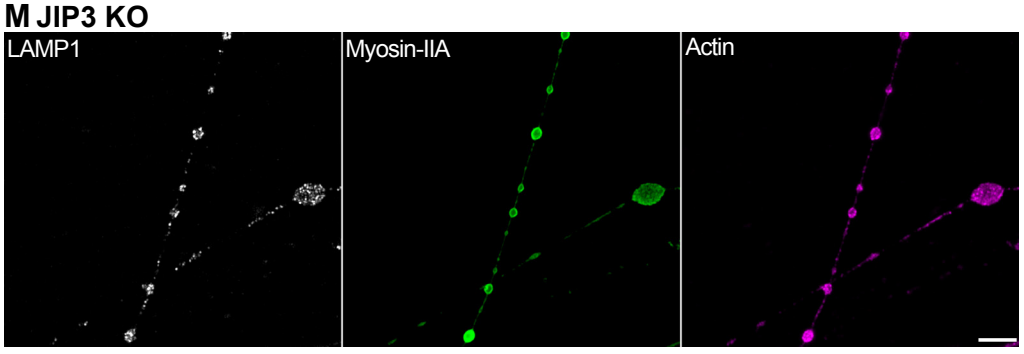

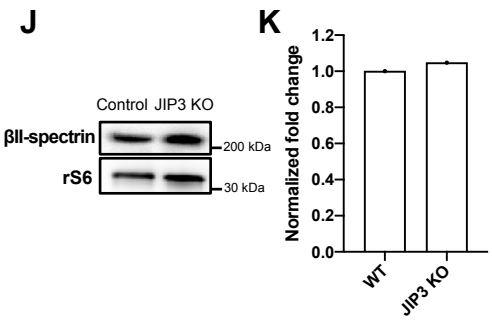

Figure 2

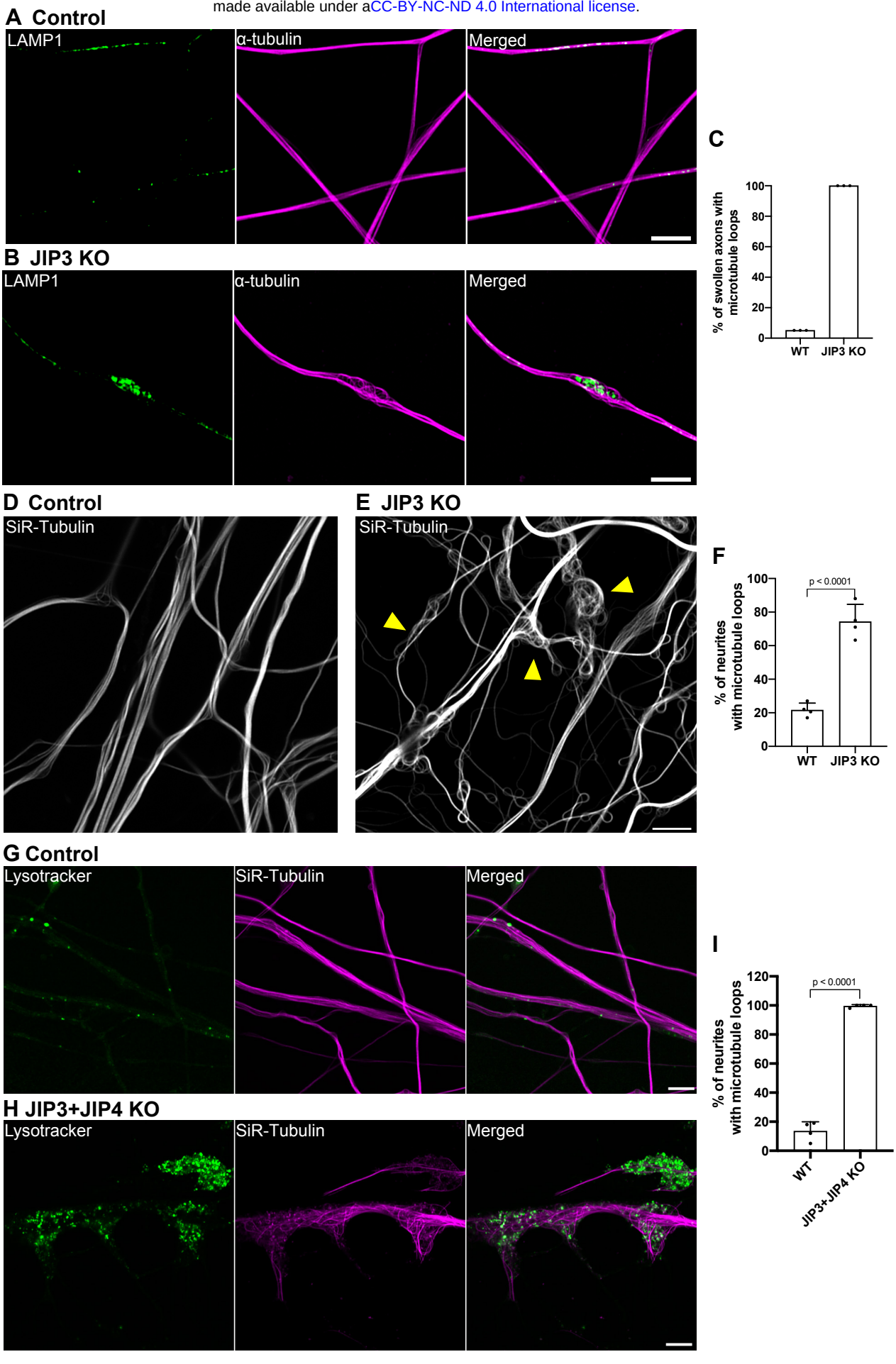

Figure 3

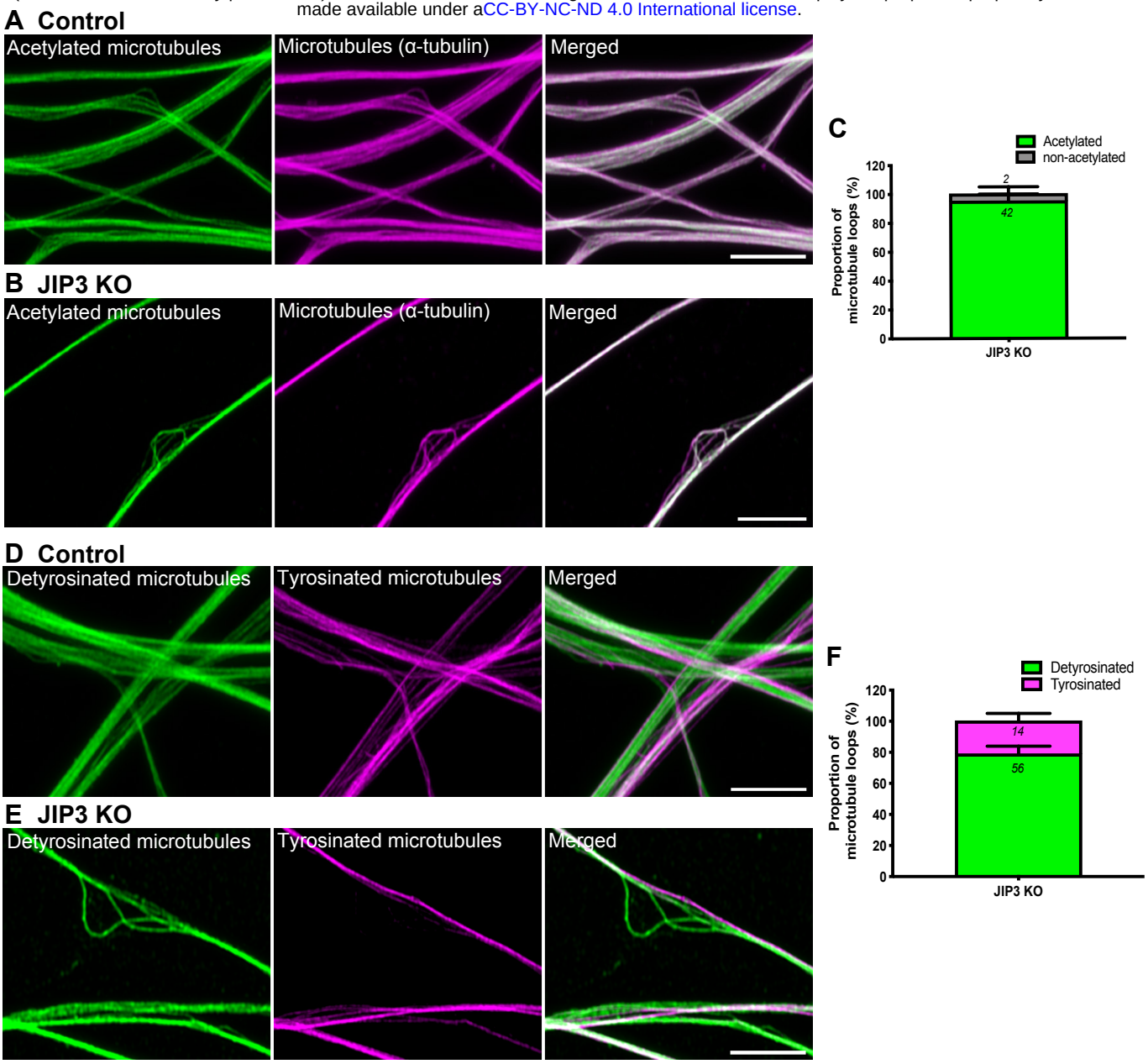

Figure 4

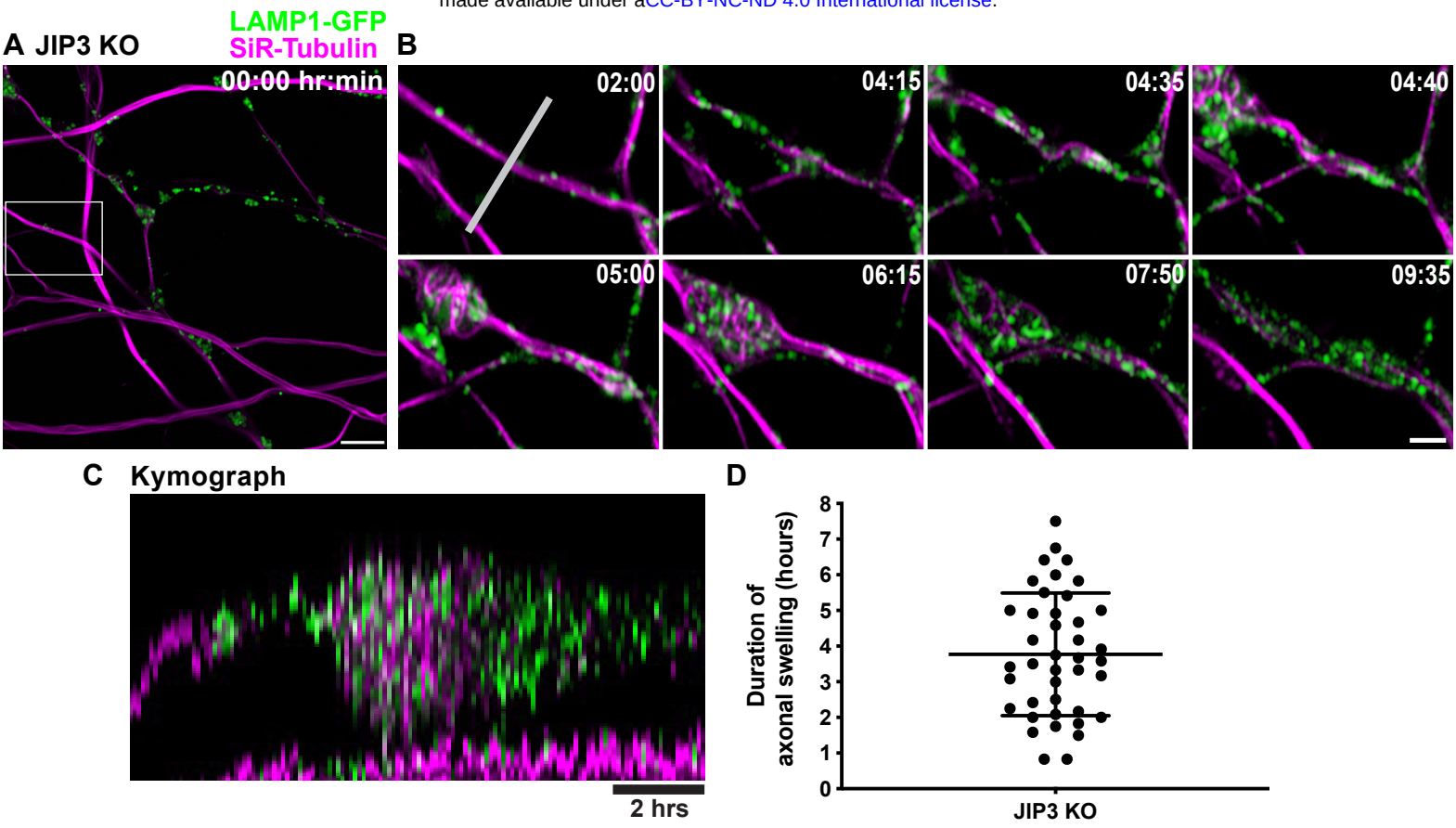

Figure 5

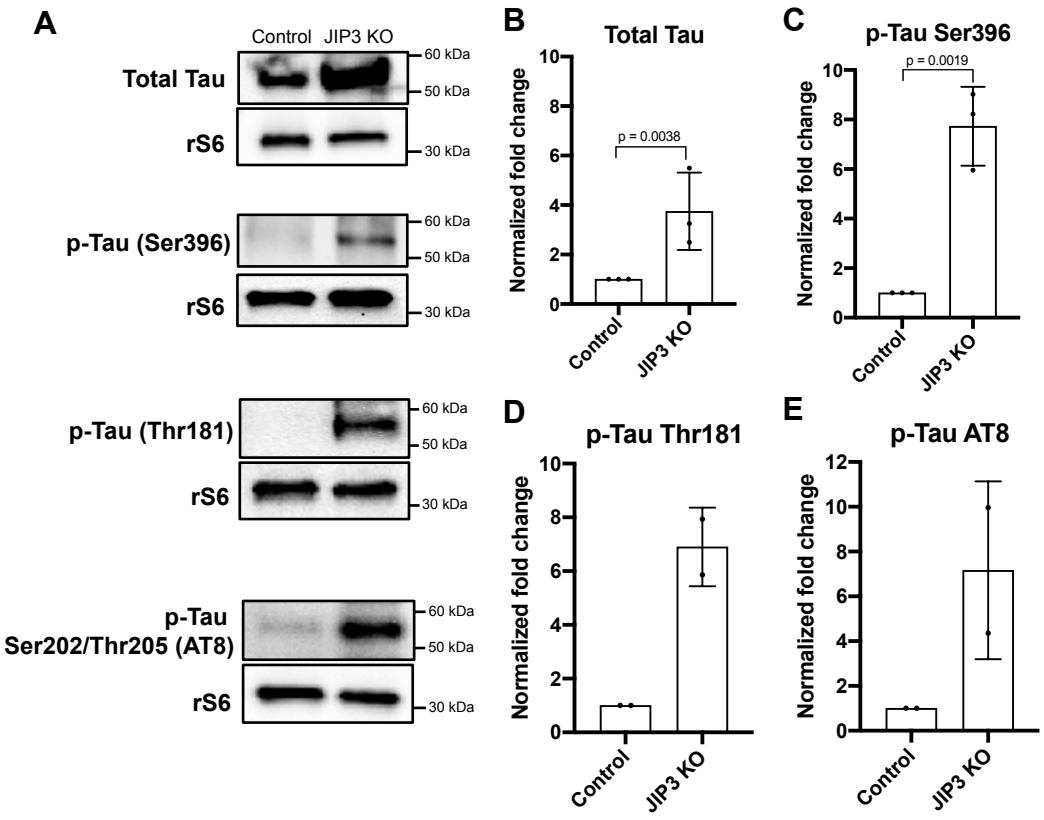

Supplementary Figure 1

A Young JIP3 KO i³Neurons with no lysosome-positive axonal swellings

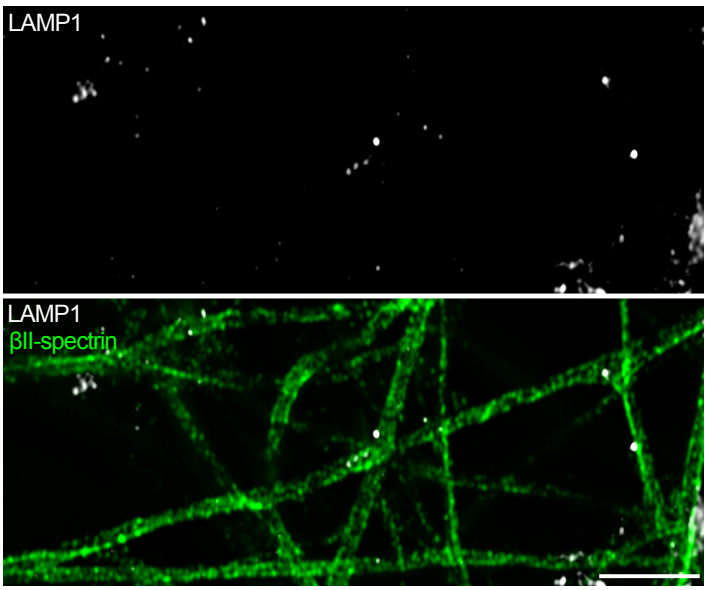

B Single neuronal swelling in an isolated JIP3 KO axon